Effect of texture on the residual stress response from laser peening of an aluminium-lithium alloy

Zabeen, S, Langer, K & Fitzpatrick, ME

Original citation & hyperlink:
Zabeen, S, Langer, K & Fitzpatrick, ME 2018, 'Effect of texture on the residual stress response from laser peening of an aluminium-lithium alloy' Journal of Materials Processing Technology, vol 251, pp. 317-329
https://dx.doi.org/10.1016/j.jmatprotec.2017.07.032

DOI 10.1016/j.jmatprotec.2017.07.032
ISSN 0924-0136

Publisher: Elsevier

Effect of texture on the residual stress response from laser peening of an aluminium-lithium alloy

S. Zabeen[1,3], K. Langer[2], and M. E. Fitzpatrick[1]

[1] *Coventry University, Faculty of Engineering and Computing, Gulson Road, Coventry CV1 2JH, UK*
[2]*Air Force Research Laboratory, Wright-Patterson Air Force Base, OH 45433, USA*
[3]*Formerly at: The Open University, Walton Hall, Milton Keynes MK7 6AA, UK*

Email: Suraiya.Zabeen@coventry.ac.uk

Abstract

Laser shock peening can improve the damage tolerance of metallic materials by introducing deep compressive residual stress that inhibits crack initiation and growth. This study investigates the laser peening of aluminium alloy in a product form – an extruded T-section – that has different crystallographic textures in different locations. The alloy studied is Al 2099, an aluminium-lithium alloy that shows anisotropy in the mechanical properties when texture is present. Specimens extracted from different regions of the extrusion were laser shock peened with a power density of 3 GW/cm^2 in single shocks as well as in a pattern arrangement. The effect of number of laser shocks on the residual stresses were characterized primarily using incremental hole drilling. The results show 20% higher residual stresses in the web area of the extrusion compared to the flange after peening with a single laser shock, with this difference decreasing as the number of shocks increases. This effect can be explained by the difference in yield strength between those locations. No significant differences were observed in the residual stresses from peening onto different planes of a textured sample at a given location.

1. Introduction

Al 2099 alloy is a third-generation aluminium-copper-lithium alloy used for aerospace structural applications, particularly in airplane internal structure and lower wing stringers. The lithium content in an Al-Li alloy increases the specific properties over traditional aluminium alloys. For example, compared to the commercially-used non-lithium Al 2024 alloy, Al 2099 shows a 5% reduction in density with 20% increase in longitudinal tensile yield strength (Giummarra, Thomas & Rioja 2007). In common with many aluminium alloys, Al 2099 shows significant in-plane and through-thickness anisotropy, particularly in the rolled products, and axisymmetric flow anisotropy in the extruded products (Rioja 1998). Generally, this anisotropy results from the strong crystallographic texture that forms during multistage thermomechanical processing. Al 2099 extruded products usually exhibit <111> + <100> fibre texture that gives a high longitudinal yield strength, with only a slight difference between the tensile yield strength the ultimate tensile strength, and low ductility

in the transverse direction (Denzer et al. 1992). Bois-Brochu *et al*. (Bois-Brochu et al. 2014) studied the effect of texture on the anisotropy of the mechanical properties of an Al 2099 extruded integrally-stiffened panel. They found a variation in mechanical properties between different locations of the panel. In all locations, the highest strength was found in the extrusion direction and the lowest strength was observed at 45° to the extrusion direction. Reductions in the yield strength of 17% and 25% were reported for the transverse and 45° directions, respectively. This anisotropic behaviour drives the design minimum strength to the 45° direction, thereby neglecting the strength benefits in other directions and taking benefit only for weight savings.

Mechanical surface treatments, such as laser shock peening (LSP), applied in appropriate orientations with respect to the extrusion direction may prove beneficial to improving the damage tolerance of anisotropic alloys. Laser shock peening introduces deep compressive residual stresses that can enhance the fatigue life of a material. The magnitude and depth of the induced residual stresses depend, among other factors, on the mechanical properties and texture of the virgin material. The level of induced residual stress is directly related to the yield stress of the material along with the hardening response.

Peening on an alloy having a significant anisotropy in mechanical properties, not only in different locations but also in different orientations, requires a thorough understanding of the influence of texture on the residual stress response due to peening. Although a substantial amount of research data is available on the effects of texture on the mechanical properties of Al 2099, very little attention has been focused on (1) the effects of LSP on residual stress generation in this alloy system, and (2) the effect of initial texture on LSP-induced residual stresses in any material. Therefore, this study investigates the effects of texture on residual stress profiles in laser peened Al 2099.

2. Material and Experimental Method

Al 2099 alloy was used in the T8 condition (solution heat treated, stretched, and artificially aged) to study the effects of texture on residual stress generation owing to LSP. Material was received from Alcoa Inc. in the form of an extruded T-bar with gross cross-sectional dimensions of 139 × 60 mm^2 and a length of 1000 mm. Figure 1 shows the T-bar geometry and the location of the regions that we refer to here as the web and flange. Test coupons with different geometries were extracted from different locations to evaluate texture, tensile strength, and residual stress after laser shock peening.

Five types of specimens were extracted from the extruded T bar for texture measurements, tensile testing, single location peening, and multiple pattern peening:

- Nine specimens with dimensions of 10 × 10 × 5 mm^3 were extracted from the web and flange sections of the extruded T-bar to study the texture variation at these locations.
- Eight longitudinal tensile specimens with geometry as shown in Figure 2 were extracted, four from the web and four from the flange, with the longitudinal axis aligned with the Z-direction of the extrusion.
- 18 samples for residual stress characterization following single peening on XY, YZ and ZX planes in three peening conditions, were extracted, nine from the web and nine from the flange. The specimen geometries are described in Table 1.
- Four specimens were used to study the effect of pattern peening on the residual stress generation XY and ZX planes, with the specimen geometries listed in Table 2.
- One specimen was used to measure the variation in hardness across the XY-plane. This specimen was a 10-mm-thick T-shaped slice of the extrusion.

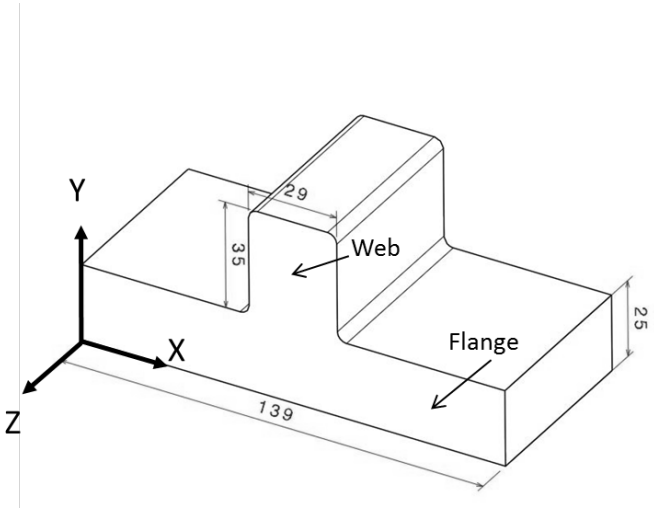

Figure 1: Specimen geometry of the extruded Al 2099 T8 T-bar showing the web and flange locations. All dimensions are in mm.

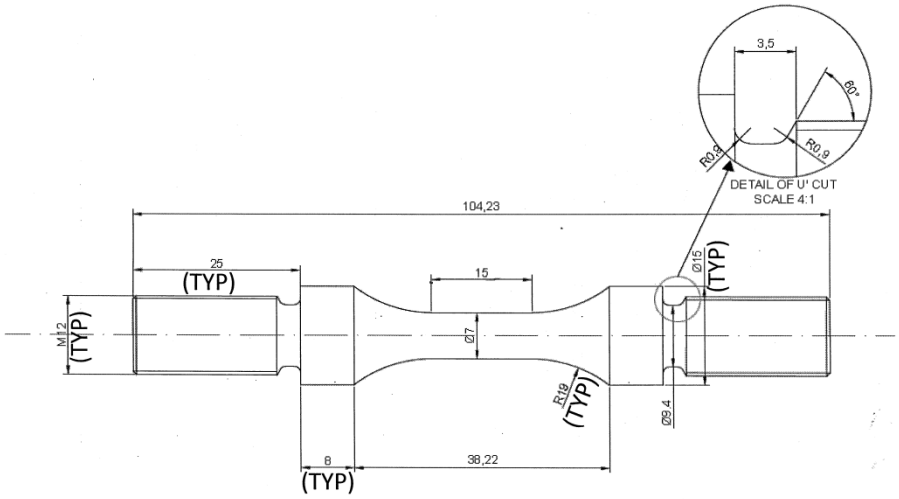

Figure 2: Specimen geometry used for tensile testing. All dimensions are in mm. M12 threads were used for fixing the samples into the test machine. The dimension of the gauge length is 15 mm.

2.1 Texture measurement using neutron diffraction

Bulk crystallograhic texture was measured using neutron diffraction at the General Materials Diffractometer (GEM) instrument at the UK's ISIS neutron source (Kockelmann, Chapon & Radaelli 2006). A beam size of 20 × 20 mm^2 was used. The recorded data were normalized to the incident neutron flux distribution, corrected for detector efficiencies, and converted to a diffraction pattern (intensity as a function of *d*-spacing). The diffraction patterns were then Rietveld fitted (Wenk, Lutterotti & Vogel 2010) in MAUD software (Lutterotti et al. 1997). The (111), (200) and (220) pole figures were plotted. An example of the fitted spectra is shown in Figure 3.

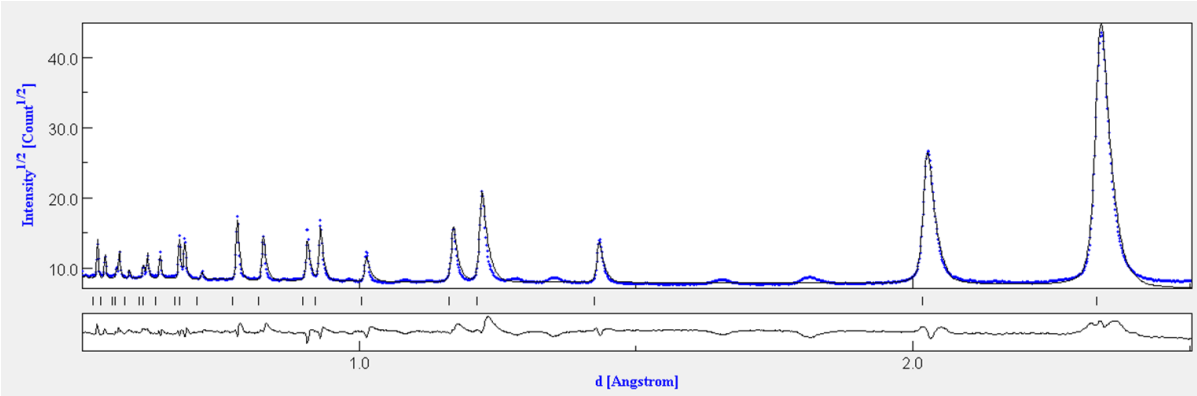

Figure 3: Neutron diffraction spectra fitting in MAUD software for the 2099 material

2.2 Hardness and Tensile Strength Tests

A hardness map was generated from the full cross-section (XY plane) of the T bar as shown in Figure 1. The surface was metallographically polished to OPS finish for Vickers hardness measurements. Indentation was carried out with a load of 5 kgF.

Tensile tests were carried out on a 50 kN Instron 3369 universal testing system, following ASTM standard E8/E8M-13a

2.3 Laser shock peening

Eighteen coupons with dimensions as shown in Table 1 were extracted from the web and flange sections of the extruded bar and peened at Metal Improvement Company (Earby, UK) using the peening parameters and geometries listed in Table 1. A 5 × 5 mm^2 laser spot with an intensity of 3 GW/cm^2 was used, with peening at the geometric centre of each test coupon as shown in Figure 4a. For multiple laser shocks, each peen spot was applied directly over the previous spot.

Four coupons with dimensions as shown in Table 2 were pattern-peened to investigate the effects of shot overlap in a more conventional peen pattern over a larger area. Two specimens were extracted from each of the web and flange locations, with one specimen from each location peened on the XY plane and the other on the ZX plane. All spots were 5 × 5 mm^2 with an intensity of 3 GW/cm^2 and a pulse width of 18 nanoseconds. Each layer of spots was formed with the individual spots applied nominally edge-to-edge (a 5% overlap was used between the spots within each layer). Three layers were used with a 50% offset between each layer (equivalent to 300% coverage).

Table 1: Single location Peening conditions

Specimen Number	Extraction location	Peened plane	Peening condition Single Spot (Notation is GW/cm^2 – ns – number of laser hits)	Specimen dimensions / mm^3
1a	Flange	YZ	3-18-1	50 × 50 × 25
2a		XY	3-18-1	
3a		ZX	3-18-1	
1b		YZ	3-18-3	
2b		XY	3-18-3	
3b		ZX	3-18-3	
1c		YZ	3-18-5	
2c		XY	3-18-5	
3c		ZX	3-18-5	
4a	Web	YZ	3-18-1	60 × 25 × 15
5a		XY	3-18-1	
6a		ZX	3-18-1	
4b		YZ	3-18-3	
5b		XY	3-18-3	
6b		ZX	3-18-3	
4c		YZ	3-18-5	

5c		XY	3-18-5
6c		ZX	3-18-5

Table 2: Multiple Pattern Peening conditions

2.3.1.1.1.1 Specimen No	2.3.1.1.1.2 Extraction location	2.3.1.1.1.3 Peened Plane	2.3.1.1.1.4 Specimen dimensions / mm^3
7C	2.3.1.1.1.5 Web	2.3.1.1.1.6 Y	2.3.1.1.1.7 6 Cimen dim
2.3.1.1.1.8 C		2.3.1.1.1.9 X	2.3.1.1.1.10 6 Cimen dim
2.3.1.1.1.11 R	2.3.1.1.1.12 Flange	2.3.1.1.1.13 Y	2.3.1.1.1.14 0 Ngeen dim
2.3.1.1.1.15 R		2.3.1.1.1.16 X	2.3.1.1.1.17 0 Ngeen dim

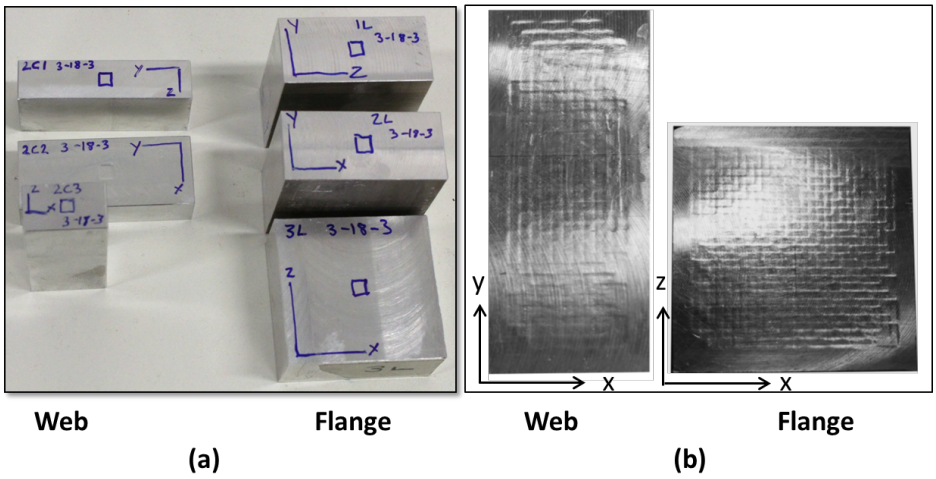

Figure 4: (a) single location peened specimens, (b) patterned peened specimens

2.4 Residual Stress Measurement by Incremental Hole Drilling

Incremental hole drilling is a relatively fast, straightforward, and inexpensive method for residual stress measurement in the laboratory. In this technique a small hole is drilled or milled into the specimen, which causes elastic strain relaxation as material is removed. The elastic strain relaxation causes a change in displacement in the surrounding material that is measured by a strain gauge attached to the specimen surface. The pre-existing residual stresses are then calculated from the measured displacements.

Hole drilling measurements were carried out using a set-up developed by Stresscraft, UK. For accurate measurements, the UK NPL Good Practice Guide No. 53 and ASTM 837 standard were followed (ASTM E837 − 13a 2013, Grant, Lord & Whitehead 2006).

A 2-mm-diameter hole was milled in an orbital motion with four depth increments of 32 µm, four depth increments of 64 µm, and eight depth increments of 128 µm for a total of 16 increments and a total depth of 1.4 mm. Strain gauge rosettes supplied by Vishay with part numbers CEA-13-062UL-120 and EA-13-062RE-120 were used.

2.5 Residual Stress Measurement by laboratory X-ray Diffraction

Residual stresses are also characterized by $\sin^2 \psi$ method (Noyan, Cohen 1987). This method measures the in-plane near-surface stresses. The measurement parameters are listed in Table 3.

Table 3: Laboratory X-ray diffraction parameters used for residual stress measurements

X-ray Tube	Cr K-α
Wavelength / nm	0.229107
2-Theta / ˚	139.3
{hkl}	311
Tilt Angles / ˚	± 45
Tilt Oscillation / ˚	5
Measuring Mode	Modified χ
Collimator Distance / mm	11.9
Collimator Diameter / mm	3

2.6 Finite Element Analysis

Finite element modelling was conducted to predict the stress and deformation states resulting from laser peening. The commercial code Abaqus/EXPLICIT 6.14-1 was used for all simulations. Each impact pulse was modelled using two distinct solution steps so that the computational parameters could be adjusted for improved efficiency and convergence. The

first solution step starts with the initial application of the pressure pulse and ends when no further plastic deformation occurs. The second solution step introduces Rayleigh damping into the model, to return the system to a state of near-equilibrium, and lasts until the kinetic energy is sufficiently damped out. One pair of analyses was performed for each laser pulse.

Because strain-rate effects on the material hardening were not available for this alloy, a simple isotropic hardening model was used. It should be noted that this assumption could lead to overprediction of compressive stresses and underprediction of the compensatory tension (Langer et al. 2015).

The pressure profile from the laser pulse was estimated using the one-dimensional model proposed by Fabbro *et al.*(Fabbro et al. 1990):

$$P_{max}(GPa) = 0.01\sqrt{\frac{\alpha}{2\alpha+3}}\sqrt{I_0\left(\frac{GW}{cm^2}\right)Z\left(\frac{g}{cm^2 s}\right)} \quad (2)$$

where α is a corrective factor corresponding to the fraction of internal energy comprised of thermal energy (typically about 0.25) (Berthe et al. 1997); I_0 is the peak power density of the laser; and Z is the effective acoustic impedance of the interface between the ablative coating and the transparent overlay, defined by:

$$\frac{2}{Z} = \frac{1}{Z_{coating}} + \frac{1}{Z_{overlay}} \quad (3)$$

Here $Z_{coating}$ and $Z_{overlay}$ are the acoustic impedances of the ablative coating and the transparent overlay, respectively. With water as the overlay ($Z \approx 0.15 \times 10^6 \mathrm{g\ cm^{-2}}$) and aluminum tape as the coating ($Z \approx 1.7 \times 10^6 \mathrm{g\ cm^{-2}}$), Z has a value of about $0.3 \times 10^6 \mathrm{g\ cm^{-2}}$. The FWHM of the pressure pulse was taken to be three times the FWHM of the laser pulse, following the observations in (Peyre, Fabbro 1995).

3. Results and Discussions

3.1 Mechanical properties

Figure 5b shows the Vickers microhardness map for a cross-section of the extruded T-bar. The result clearly shows a hardness variation within and between the web and the flange sections. In the flange, a hardened surface layer with a thickness of 2 mm at the top surface and 1 mm at the bottom surface is observed. These outer regions are approximately 18% harder than the central section of the flange. The hardness of the web section is about 140 HV5 (Vickers Hardness), which is similar to the hardness of the skin layer in the flange.

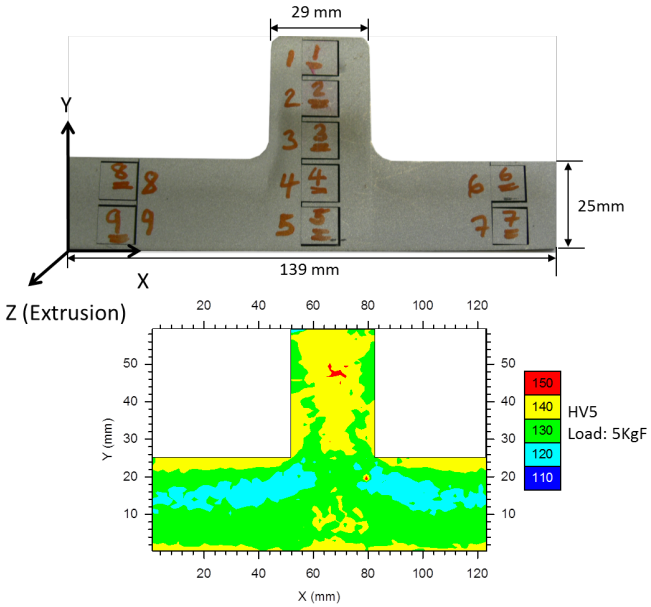

Figure 5: (a) Specimen Geometry of the extruded bar showing the axis system used; (b) corresponding Vickers microhardness map in XY orientation.

Figure 6 shows tensile test results for specimens extracted from the web and flange sections, with gauge length parallel to the Z-axis as shown in figure 5a. Results from four specimens were averaged. Specimens extracted from the web location show 38% higher yield stress than the specimens extracted from the flange section (Table 4). Higher UTS is also found in the web compared to the flange. A comparison of mechanical properties between the web and flange specimens is shown in Table 4. Also plotted in Figure 6 the stress-strain curve for a conventional Al-Cu alloy for comparison.

Table 4: Mechanical properties of Al 2099 alloy

Material	Elastic Modulus/GPa	Yield Strenght σ_y / MPa	E/σ_y	Ultimate Tensile Strength/MPa	Elongation/%
Al-2099 Web	70	575	122	617	8.6
Al-2099 Flange	70	414	169	536	8.6
Al-2624 T39	70	460	152	487	15

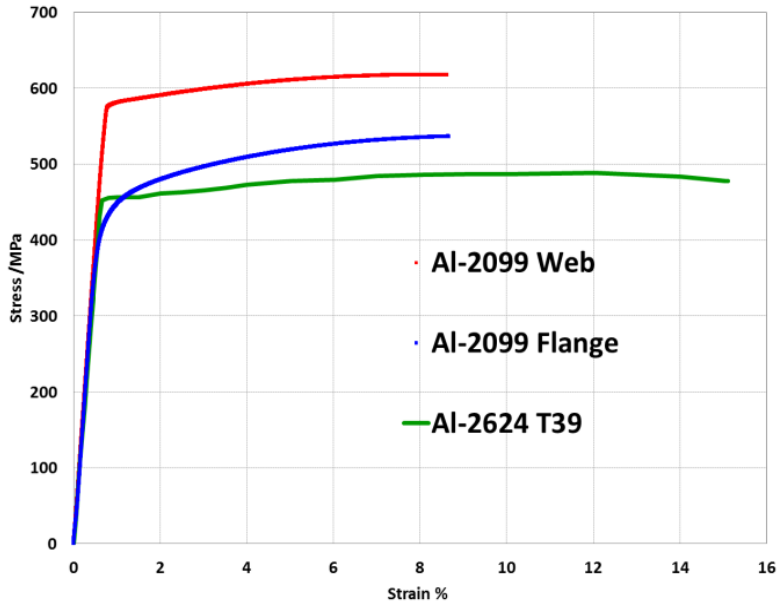

Figure 6: Engineering stress-strain curves for the web and flange material, plus data from Al 2624 for comparison (source of data?)

3.2 Macrotexture and Microstructural evolution

Preferred crystallographic orientation or texture results in anisotropic mechanical properties in polycrystalline material. Al-Li extrusion products show in-plane and through-thickness texture variation, and also a texture difference between the web and flange sections of extruded T-bar (Hales, Hafley 1998).

Figure 7 presents the reconstructed (111), (200) and (220) pole figures for the specimens extracted from different locations in the extrusion as shown in Figure 5a. Specimens 1, 2 and 3 (extracted from the web) show typical <111> fibre texture, consistent with what has been reported in the literature (Denzer et al. 1992, Jata, Singh 2014). The intersection of the flange and the base of the web (specimen 5) has a rolling-type texture. A weak rolling type texture can also be observed in specimens 6 and 7.

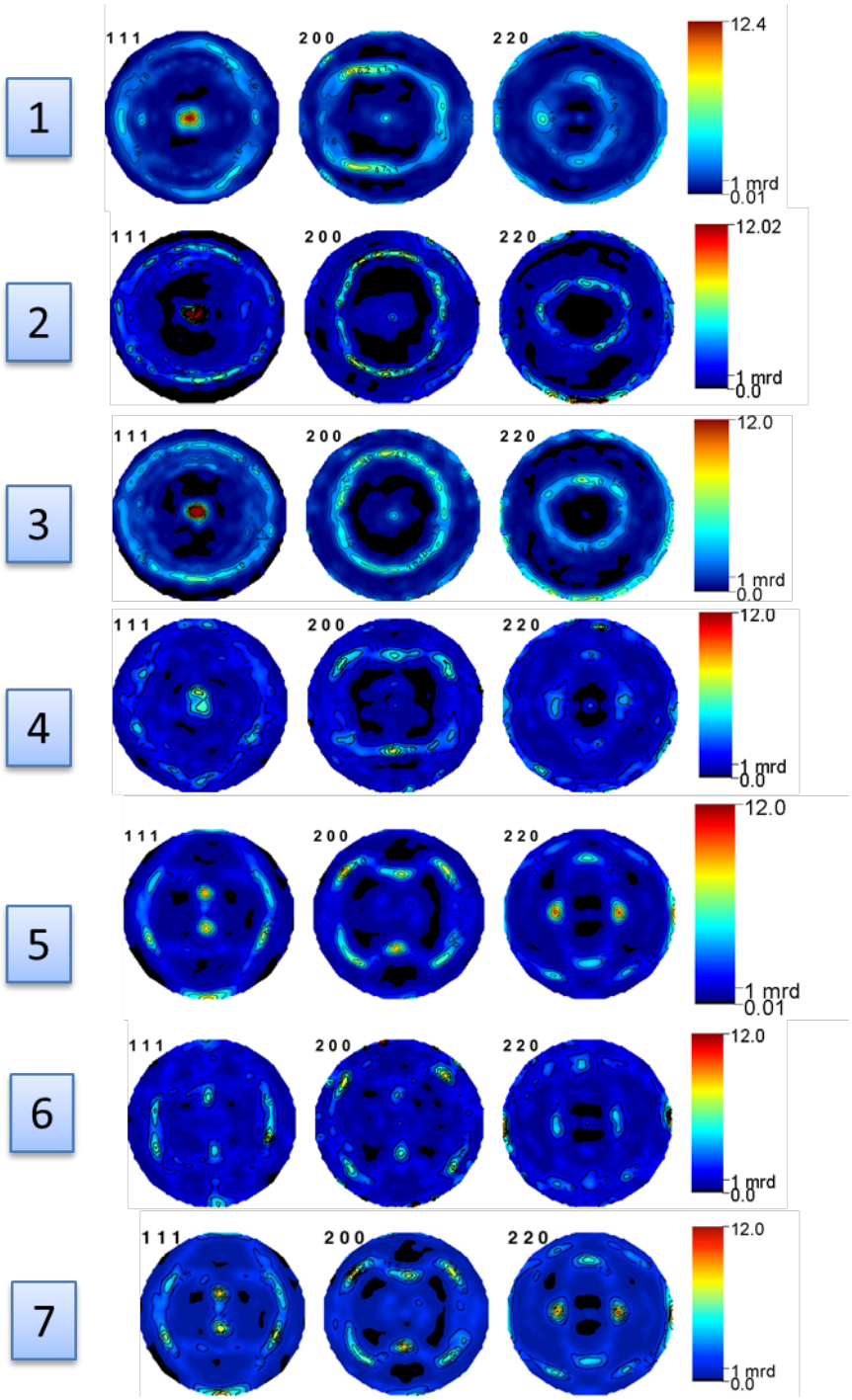

Figure 7: (111), (200), and (220) pole figures for specimens 1 to 7 as shown in Figure 5.

3.3 Surface Profile of the Single Peened Specimens

Figure 8a and b show the surface profiles of single-spot peened web (specimen 5b) and flange (specimen 2b) specimens, respectively (with conditions 3 GW cm^{-2} for 18 ns, and three sequential shocks, 3-18-3, onto the XY plane). An uneven depression from the peening is evident in both specimens. This may be a result of a non-uniform energy distribution across the laser spot. This phenomenon is not uncommon in laser peening (Dorman et al. 2012, Hfaiedh et al. 2015, Toparli 2012). For this reason, in typical industrial

applications, multiple layers of peening with overlap of the shots is used to achieve a more uniform surface profile as well as residual stress.

A horizontal line profile through the centre of the peen spot was extracted from the contour data and compared with similar line plots from peening on the YZ and ZX planes (Figures 8c and d). A maximum depth of about 30-40 µm is observed for the web specimen, with a pile up at the peen boundary of about 15-25 µm, as shown in Figure 8c. Similar results are found for the flange specimens, Figure 8d. The difference in the depression depth between XY, YZ, and ZX orientations is very small for both web and flange locations.

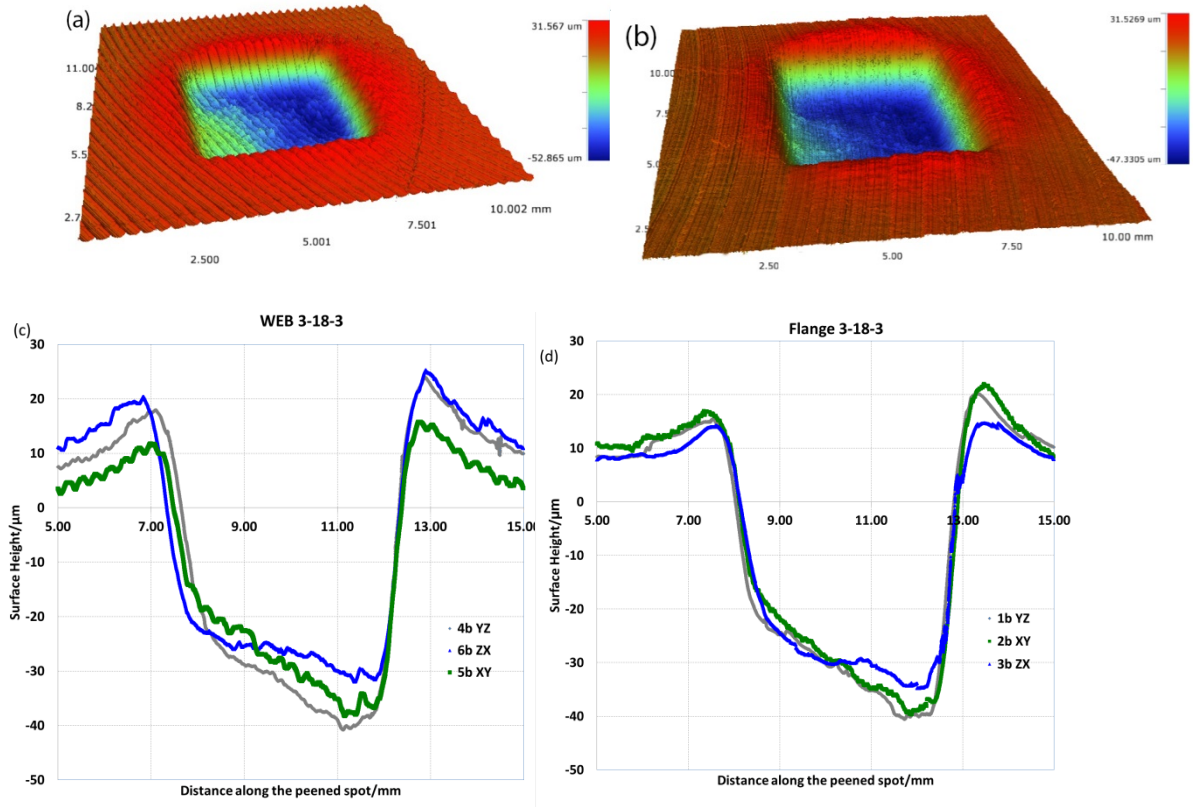

Figure 8: Surface profile for single-location peened specimens for (a) and (c) the web, and (b) and (d) the flange locations after peening at 3-18-3; (c) and (d) compare the surface line profiles for peening on the XY, YZ, and ZX planes.

3.3.1 Comparison with the numerical prediction

Figure 9 presents a comparison between predicted and experimental surface profiles for the single-location peened specimens with 3-18-3 peening conditions. The predicted surface profile for the flange compares well with the experimental surface profile, with a maximum depression depth of about 40 µm. However, for the web, the model predicts a lower depth (20 µm) compared to the measured surface profile. The higher yield stress used to model the web response generated a lower deformation depth than is observed experimentally. It is also to be noted that the profiles of the peened spot vary significantly between the prediction and the experimental result. During laser peening the material undergoes high-strain-rate deformation, and the type of hardening experienced by the alloy cannot be predicted (Langer *et al*. 2016). Whilst the model did not take account of the

hardening and associated high-strain-rate effects, the depression depth was predicted relatively accurately for the flange. It can be concluded that strain hardening plays an important role in the softer material with lower strength.

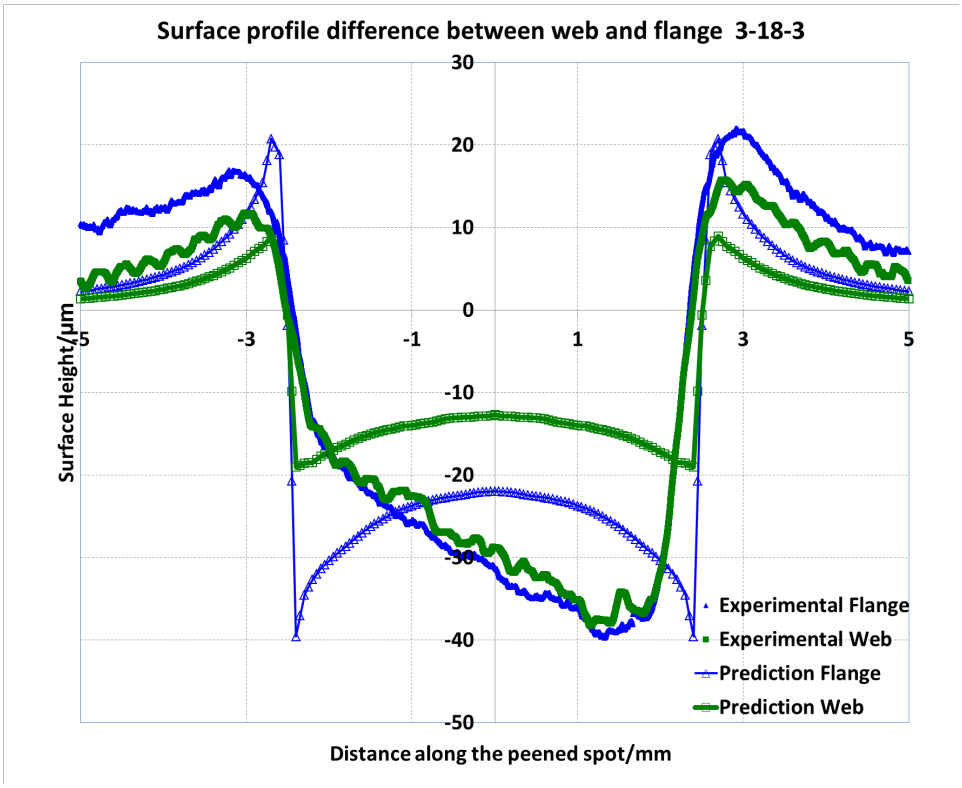

Figure 9: Comparison of surface profiles of single location peened specimen (experimentally measured and predicted).

3.4 Residual Stress

Figure 10a and 10b compare the residual stress distributions as a function of orientation for the 3-18-1 peening condition for specimens extracted from the web and flange, respectively. Two in-plane stress components were determined. After a single laser shock exposure the near-surface residual stresses in the web specimens are in the range of –75 to –200 MPa (Figure 10a); under the same peening conditions, the measured stresses in the flange specimens are in the range of –100 to –150 MPa (Figure 10b). A similar level of surface stress is reported in (Hfaiedh et al. 2015) for single location peening of a similar aluminium-lithium alloy, Al 2050-T8, with an energy of 3.5 GW/cm^2 for 10 ns using a 1.5 mm diameter circular spot; however, the depth at which balancing tensile stress appears is reported as 675 µm, whereas for our samples at this depth, as shown in Figure 10a, –200 MPa stress is still present. This may be due to the shorter pulse length – and hence lower energy – that they used. There does not seem to be a significant variation in the residual stresses between the XY, YZ, and ZX orientations in either the flange or web specimens.

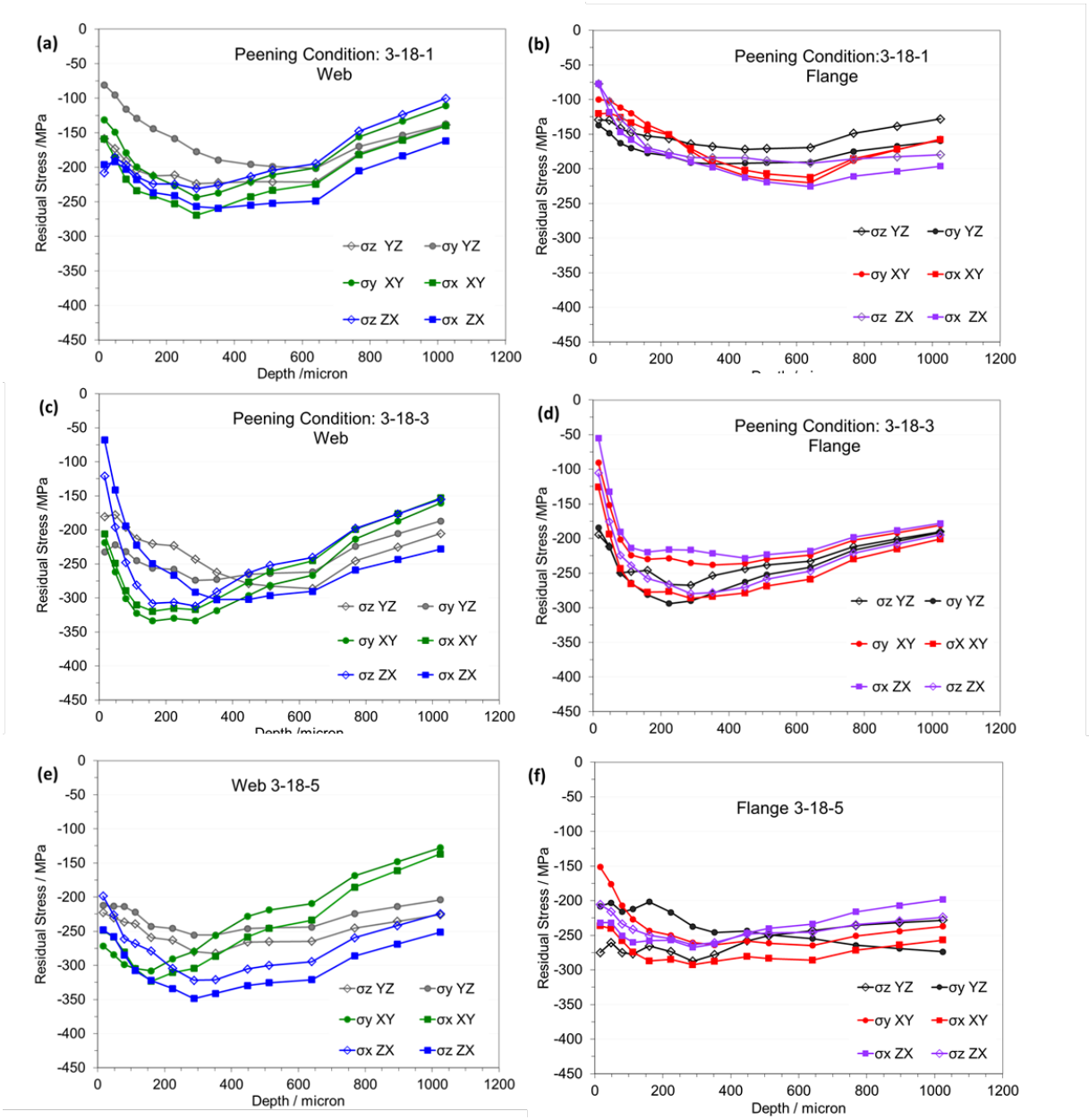

Figure 10: Comparison of residual stress profiles between (a), (c), (e) the web and (b), (e), (d) the flange after laser peening with one, three and five successive shock exposures respectively at a peening energy of 3 GW/cm^2. The difference in residual stress between peening on the XY, YZ and ZX planes of the specimens are also shown.

Figure 10c and 10d show similar residual stress measurements for specimens exposed to three layers of peening (the 3-18-3 condition). No noticeable difference seems to be evident in the residual stress profiles between the orientations within the bounds of scatter in the data, in both the web as well as the flange. The maximum compressive residual stresses for the web and the flange are –330 MPa and –300 MPa. ~~in the range of –240 to –290 MPa. However, the σ_x and the σ_y components of stress for peening onto the XY plane are slightly higher in magnitude than the corresponding stress components in the other two orientations. While peening on the XY plane, the laser-induced shock wave acts along the~~

~~extrusion direction, which has the greater yield strength than the transverse (X) direction. This may be the reason why a higher value of residual stresses is observed for peening on this plane. In the flange section little differences in the residual stress were observed between XY, YZ and ZX plane due to lower texture.~~

Residual stress distributions after five successive laser shocks are shown in Figures 10e and 10f for the web and flange specimens, respectively. The maximum compressive residual stress in the web is about –350 MPa, with slightly less compression observed in the flange (about –300 MPa). Following 5 hits the residual stresses remained largely unchanged showing strain hardening saturation. ~~some effects of orientation are observed in the web specimens, with no noticeable effects observed in the flange~~. The residual stresses obtained from incremental hole drilling are verified with the results from laboratory X-ray diffraction as shown in Table 5. A good correlation exists between the results from the two techniques.

Table 5: Comparison of residual stresses measured by hole drilling and laboratory X-ray diffraction for specimens peened with 3-18-5

Specimen Id and peen plane	Location	Residual stress: Incremental Hole Drilling / MPa		Residual stress: X-ray diffraction / MPa	
		σ_x	σ_Y	σ_x	σ_Y
1C YZ	Web	–223	–212	–195	–222
2C XY		–272	–249	–236	–229
3C ZX		–198	–248	–218	–268
4C YZ	Flange	–275	–208	–264	–214
5C XY		–151	–236	–163	–232
6C ZX		–232	–206	–267	–250

Figure 11 presents the FEA simulated residual stress results for the 3-18-3 peening condition. To model the residual stresses in the web and flange, the corresponding experimentally-determined yield strengths of 575 and 414 MPa were used. Comparing Figures 11a and 11b, it is evident that a relatively uniform layer of surface compressive residual stress (–375 MPa) is generated in the web as compared to the flange. A balancing tensile stress of 100 MPa appeared for both specimens. The extent of the residually-stressed region in the web is slightly smaller than in the flange in both width and depth. This observation is further clear in Figure 11c, which shows that although in the web the predicted value of maximum compressive residual stress is only 30 MPa higher than was predicted in the flange, the depth at which the maximum compressive residual stresses appear are significantly different: 0.2 mm for the web and 1 mm for the flange. A similar difference can also be seen in the location of balancing tensile stresses. This is simply because the higher yield strength of the web material causes a resistance to plastic

deformation during the shock wave propagation. The depths of the compressive residual stresses for the web and flange are 2.5 and 3.2 mm, respectively. Note that only a simple isotropic hardening model was used for prediction.

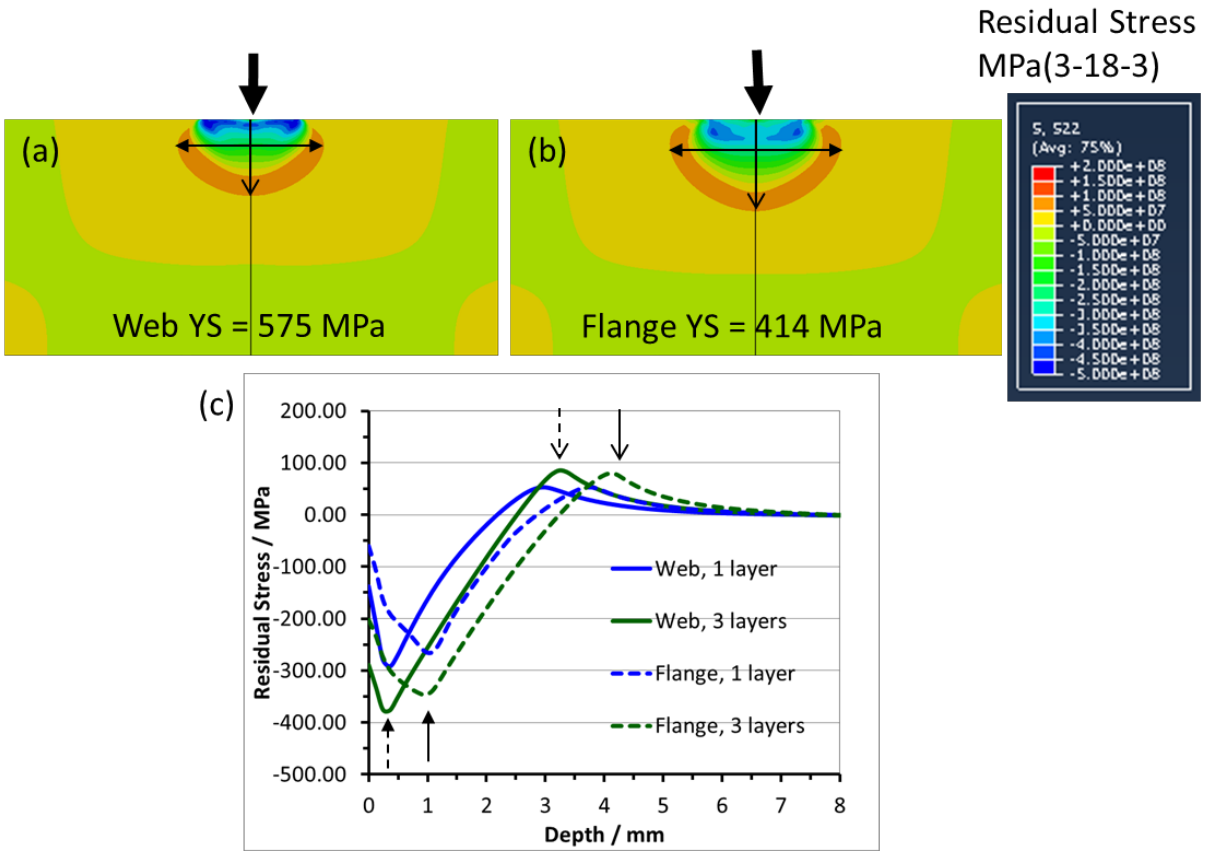

Figure 11: FEA prediction of residual stress for peening condition of 3-18-3: (a) web and (b) flange, (c) the line profiles extracted from the 2D plots and compared with the residual stresses for peening at 3-18-1.

3.5 Comparison of measured and predicted residual stress

Figure 12a and 12b show the comparison between predicted and experimental residual stress profiles in the web and flange specimens. The figures also compare residual stresses generated after 1 and 3 shocks. In agreement with the experimental results, lower levels of residual stress are predicted for 1 shock. By increasing the number of shocks from 1 to 3, approximately 100 MPa higher compressive residual stresses were introduced for both locations.

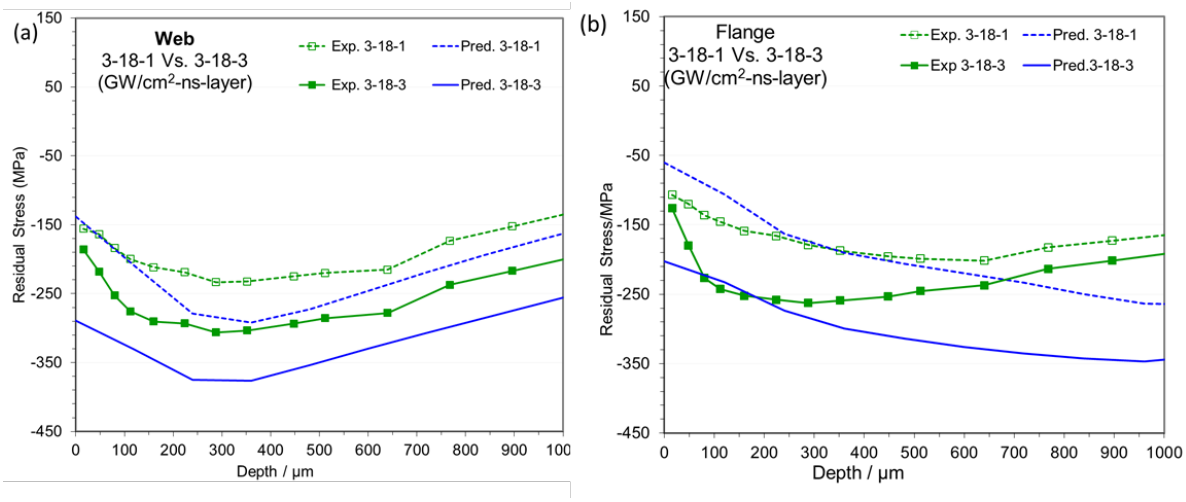

Figure 12: Comparison of predicted (blue lines) and measured (green lines) residual stresses after 1 and 3 shocks, for (a) web and (b) flange location. From Figure 12, it is clear that the model prediction of a difference of around 70 MPa in the surface stress for 1 and 3 shocks is different from that seen experimentally, where the near-surface stresses are within 20 MPa for 1 and 3 hits. Better agreement is seen for the modelling of the single shock. There is some reverse yielding near the surface, the prediction of which requires detailed knowledge of the cyclic hardening when three shocks are used. This is the subject of further work on the refinement of the model performance.

3.6 Effect of number of peen layers

Figure 13 shows the effect of the number of peen layers (the number of shocks at each location) on the residual stress distribution for peening onto the XY orientation for (a) a web specimen and (b) a flange specimen. For the flange specimen, the surface residual stress was measured to be about –100 to –125 MPa, regardless of the direction of the stress component or the number of layers. However, considering the subsurface distribution of residual stress, the magnitude of the maximum compression increases significantly as the number of peen layers increases. The maximum value of compression after 3 laser shots reached about –275 MPa at a depth of 300 µm.

The effects were more pronounced in the web specimens, with significantly higher compression after three shocks than after one. The surface residual stresses after one and three layers of peening were about –140 and –255 MPa, respectively; the maximum compressive residual stress after one and three layers of peening were about –250 and –375 MPa, respectively. The values of the compressive residual stresses are greatly increased with increasing number of peen layers; however, as is shown, the overall shape of the residual stresses profiles are similar.

Figure 14 shows a linear increase in the depth of the surface depression (peak-to-valley distance) after peening as the number of layers is increased. No difference between the peening of the flange and web regions can be detected. It is interesting to note here that

even though there is a strength variation between web and flange, no variation in the depression depth is observed. Also, the linear relationship between number of layers and the depression depth does not correlate with the measured changes in the residual stress.

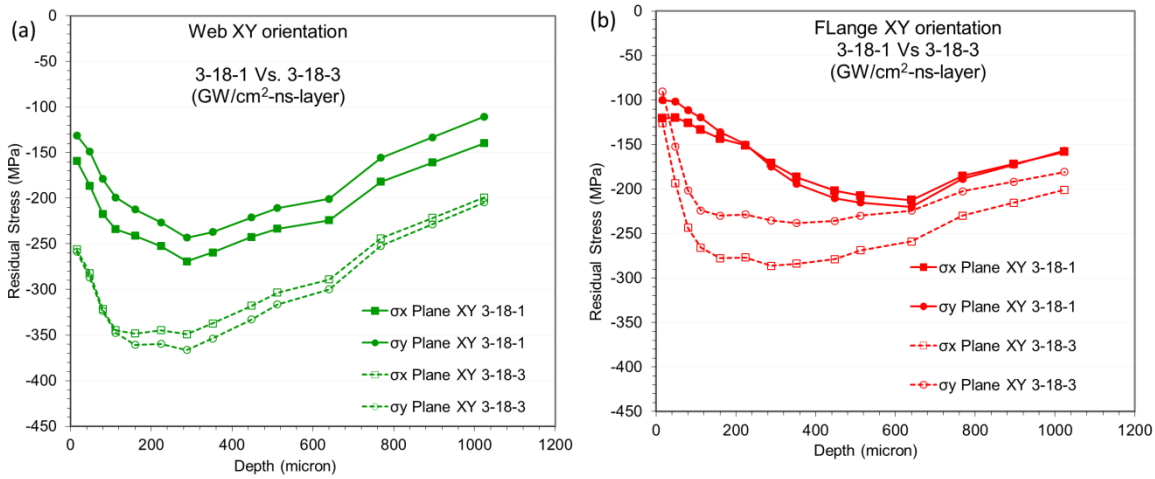

Figure 13: Effect of number of peen layers on the residual stress profiles in (a) flange and (b) web.

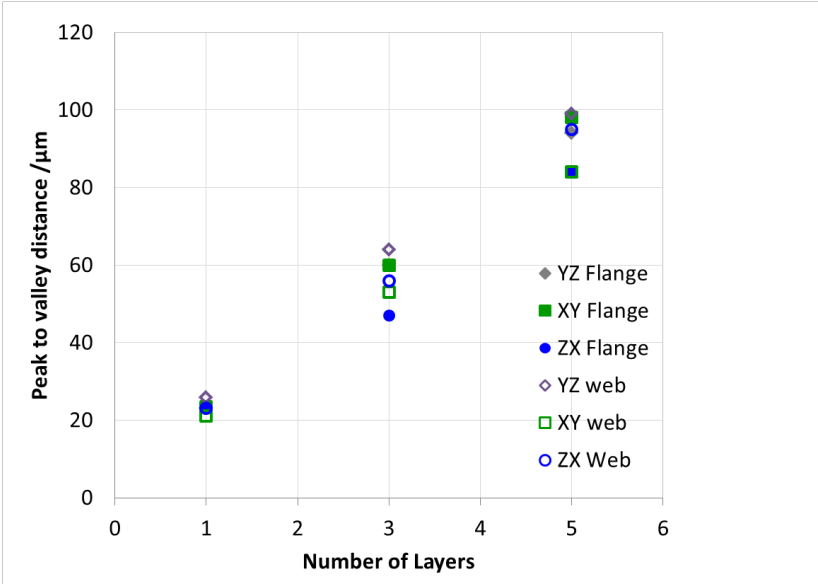

Figure 14: Effect of number of layers on the depression depth for single location peening at 3 GW/cm^2

3.7 Residual stresses from pattern peening

Surface residual stresses were measured by laboratory X-ray diffraction for a specimen, as shown in Figure 1, that was peened over the entire XY surface. The results are presented in Figure 15a and 15b for the σ_x and σ_y components, respectively. The σ_x component of the residual stress in the flange is less compressive than the stress measured in the web. This can be attributed simply to the fact that the web has a higher yield stress than the flange: *i.e.*, it is not necessary to invoke the differences seen in the texture in order to explain the result. Also note that for both the web and flange sections, the σ_x component of the

residual stress is generally less compressive than the σ_y component. Line plots (Figure 15c and 15d) are extracted from the 2D residual stress maps from peening on the XY plane and compared to the surface residual stresses measured from peening on the ZX plane. There is no significant difference in residual stress between peening on the XY and ZX planes, with the residual stresses being fairly scattered over the central 18 mm of the web section. The magnitude of the maximum compressive residual stress (about –300 MPa) generated in the web section for the σ_y component is of the same order of the compression generated in the flange section, but the σ_x component is lower in the flange section at around –200 MPa. Balancing tensile residual stresses were found at the edges of both web and flange.

Because the laboratory X-ray measurements only provide near-surface residual stress, incremental hole drilling was used to characterise the sub-surface residual stress. A comparison of residual stress from peening on the XY and ZX planes is presented in Figure 16. For the web specimens (Figure 16a) a maximum compression of about –300 MPa is generated at a depth of 290 μm. For the XY orientation the σ_x stress component has slightly lower stress than the σ_y component. In the flange specimens, the stresses resulting from peening on the XY plane are about 15% less compressive than those generated from peening on the ZX plane. This result is consistent with the X-ray measurements.

Al alloys generally show strain hardening effects. When the specimens were peened with a single shock exposure, a clear difference in residual stress was observed between the web and flange. In the web 30% higher residual stresses (calculated by averaging residual stress values in all directions at 288 μm depth) are generated than the flange, which correlates well with the fact that the web has 38% initial higher yield strength. It is interesting to note that the difference disappears for 3 or 5 shock exposures at the same depth. The most likely reason for this is that multiple shocks have caused strain hardening saturation. The results from the pattern-peened specimens reconfirm this fact, as minimal difference is observed between the web and flange, with the only exception being the stresses from peening on the XY plane.

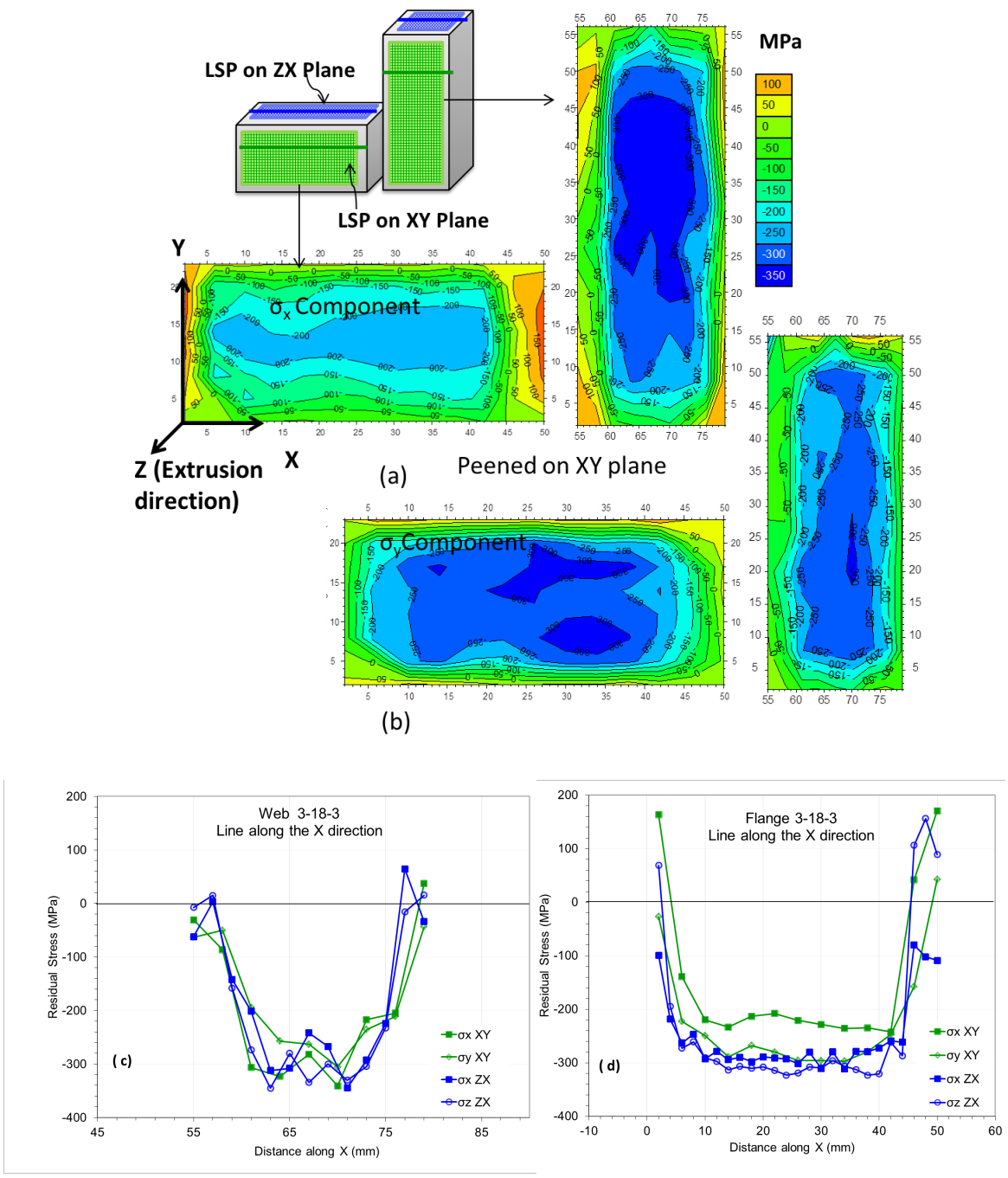

Figure 15: Surface residual stresses for pattern peened specimens (a) σ_x component following peening on the on the XY plane, (b) σ_y component following peening on the XY plane; line profile of stress with position along the X-axis in the (c) web and (d) flange showing the comparison residual stresses between XY and ZX plane. The uncertainty in these residual stress results lie within ± 25 MPa.

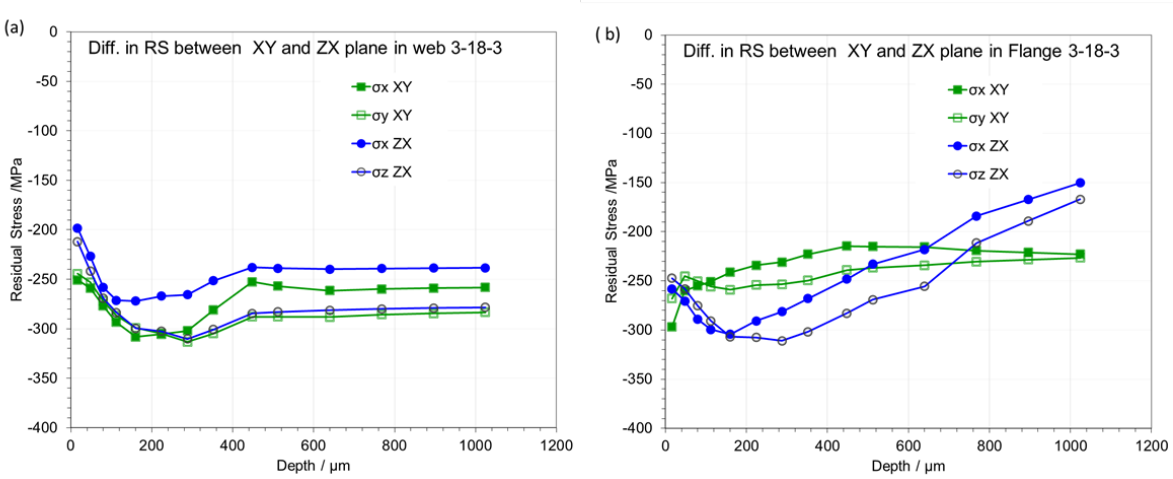

Figure 16: Depth-resolved residual stress profile measured by incremental hole drilling showing the comparison between two orientations in the (a) web and (b) flange. The uncertainty in these residual stress results lie within ± 15 MPa.

Conclusions

Laser peening was applied to different locations of an al 2099 extruded T-section, to study the effects of texture on the residual stress generation.

1. The extruded Al 2099 T–section shows a variation in strength between different locations, with the web having 38% higher yield strength than the flange. This correlates with the different crystallographic textures seen across the section, with a <111> + <100> fibre texture in the web sections.
2. After laser peening with single shots onto the same location, the residual stress induced in the web is about 25% more compressive than in the flange specimens. However, the difference in induced residual stresses is greatly minimized after multiple laser shocks owing to strain hardening and strain hardening saturation. The differences in residual stresses for identical peening in different locations can be linked to the difference in baseline mechanical properties that arises in the different regions of the extrusion.
3. No significant variation in the residual stress could be detected between peening onto samples from different orientations when a strong texture is present.
4. A good agreement was found between the experimental and numerically predicted residual stress profiles; however, the models could not accurately predict the

surface deformation. This is likely because the numerical model idealizes the distribution of energy across the laser and does not account for nonuniformity.

5. Pattern peening in the web and flange sections induced similar levels and distributions of compressive residual, suggesting that the beneficial effects of layering can overcome variations in the mechanical properties of a given alloy as a result of thermomechanical processing.

It can be concluded that laser peening of formed aluminium products must take into account of local differences in properties. Forgings and extrusions will have different textures and yield stress in different locations, and will therefore have different level of induced residual stress. The difference in residual stresses can be rationalised solely in terms of the elastic-plastic properties: no effects of texture *per se* were observed.

Acknowledgements

This research effort was sponsored by the Air Force Office of Scientific Research, Air Force Material Command, USAF, under grant number FA8655-12-1-2084, and the Air Force Research Laboratory's Aerospace Vehicles Directorate. The U.S. Government is authorized to reproduce and distribute reprints for Government purpose notwithstanding any copyright notation thereon. The views and conclusions contained herein are those of the authors and should not be interpreted as necessarily representing the official policies or endorsements, either expressed or implied, of the Air Force Office of Scientific Research or the U.S. Government. The authors would like to thank Dr Markus Heinimann at Alcoa Inc. for the provision of the material studied in the project. Thanks are also due to Dr Andy Fitch at ESRF, Grenoble, France; Dr Winfried Kockelmann, ISIS, UK; Mr Pete Ledgard and Mr Stan Hiller at The Open University, and Dr Philip Whitehead at Stresscraft, UK for technical support. MEF is grateful for funding from the Lloyd's Register Foundation, a charitable foundation helping to protect life and property by supporting engineering-related education, public engagement and the application of research.

4. References

ASTM E837 – 13a 2013, *Standard Test Method for Determining Residual Stresses by the Hole-Drilling StrainGage Method1*, ASTM International, 100 Barr Harbor Drive, PO Box C700, West Conshohocken, PA 19428-2959. United States.

Berthe, L., Fabbro, R., Peyre, P., Tollier, L. & Bartnicki, E. 1997, "Shock waves from a water-confined laser-generated plasma", *Journal of Applied Physics,* vol. 82, no. 6, pp. 2826-2832.

Bois-Brochu, A., Blais, C., Goma, F.A.T., Larouche, D., Boselli, J. & Brochu, M. 2014, "Characterization of Al–Li 2099 extrusions and the influence of fiber texture on the anisotropy of static mechanical properties", *Materials Science and Engineering: A,* vol. 597, no. 0, pp. 62-69.

Denzer, D.K., Hollinshead, P.A., Liu, J., Armanie, K.P. & Rioja, R.J. 1992, "Texture and Properties of 2090, 8090 and 7050 Extruded Products, Ibid. (II) (1992), pp.903.", *VI International Aluminium-Lithium Conference,* vol. ii, pp. 903-909.

Dorman, M., Toparli, M.B., Smyth, N., Cini, A., Fitzpatrick, M.E. & Irving, P.E. 2012, "Effect of laser shock peening on residual stress and fatigue life of clad 2024 aluminium sheet containing scribe defects", *Materials Science and Engineering: A,* vol. 548, no. 0, pp. 142-151.

Fabbro, R., Fournier, J., Ballard, P., Devaux, D. & Virmont, J. 1990, "Physical study of laser-produced plasma in confined geometry", *Journal of Applied Physics,* vol. 68, no. 2, pp. 775-784.

Giummarra, C., Thomas, B. & Rioja, R.J. 2007, "New aluminum lithium alloys for aerospace applications. In *Proceedings of the light metals technology conference*.", *light metals technology,* .

Grant, P.V., Lord, J.D. & Whitehead, P. 2006, *The Measurement of Residual Stresses by the Incremental Hole Drilling Technique - Issue 2*, The National Physical Laboratory (NPL).

Hales, S.J. & Hafley, R.A. 1998, "Texture and anisotropy in Al-Li alloy 2195 plate and near-net-shape extrusions", *Materials Science and Engineering: A,* vol. 257, no. 1, pp. 153-164.

Hfaiedh, N., Peyre, P., Song, H., Popa, I., Ji, V. & Vignal, V. 2015, "Finite element analysis of laser shock peening of 2050-T8 aluminum alloy", *International Journal of Fatigue,* vol. 70, no. 0, pp. 480-489.

Jata, K.V. & Singh, A.K. 2014, "Chapter 5 - Texture and Its Effects on Properties in Aluminum–Lithium Alloys" in *Aluminum-lithium Alloys*, eds. N.E. Prasad, A.A. Gokhale & R.J.H. Wanhill, Butterworth-Heinemann, Boston, pp. 139-163.

Kockelmann, W., Chapon, L.C. & Radaelli, P.G. 2006, "Neutron texture analysis on GEM at ISIS", *Physica B: Condensed Matter,* vol. 385–386, Part 1, no. 0, pp. 639-643.

Langer, K., Olson, S.E., Brockman, R.A., Braisted, W.R., Spradlin, T. & Fitzpatrick, M.E. 2015, *High Strain-Rate Material Model Validation for Laser Peening Simulation*, iet.

Lutterotti, L., Matthies, S., Wenk, H.-., Schultz, A.S. & Richardson, J.W. 1997, "Combined texture and structure analysis of deformed limestone from time-of-flight neutron diffraction spectra", *Journal of Applied Physics,* vol. 81, no. 2, pp. 594-600.

Noyan, I.C. & Cohen, J.B. 1987, *Residual Stress - Measurement by Diffraction and Interpretation.* Springer-Verlag, Berlin.

Peyre, P. & Fabbro, R. 1995, "Laser shock processing: a review of the physics and applications", *Optical and Quantum Electronics,* vol. 27, no. 12, pp. 1213-1229.

Rioja, R.J. 1998, "Fabrication methods to manufacture isotropic Al-Li alloys and products for space and aerospace applications", *Materials Science and Engineering: A,* vol. 257, no. 1, pp. 100-107.

Toparli, M.B. 2012, *Analysis of Residual Stress Fields in Aerospace Materials After Laser Peening*, The Open University.

Wenk, H.-., Lutterotti, L. & Vogel, S.C. 2010, "Rietveld texture analysis from TOF neutron diffraction data", *Powder Diffraction,* vol. 25, no. 03, pp. 283-296.